THE JOURNAL OF PHYSICAL CHEMISTRY A

Article

pubs.acs.org/JPCA

Mechanism of Co−C Bond Photolysis in Methylcobalamin: Influence of Axial Base

Piotr Lodowski,[†] Maria Jaworska,[†] Brady D. Garabato,[‡] and Pawel M. Kozlowski*[,‡]

[†]Department of Theoretical Chemistry, Institute of Chemistry, University of Silesia, Szkolna 9, PL-40 006 Katowice, Poland

[‡]Department of Chemistry, University of Louisville, Louisville, Kentucky 40292, United States

Supporting Information

ABSTRACT: A mechanism of Co−C bond photolysis in the base-off form of the methylcobalamin cofactor (MeCbl) and the influence of its axial base on Co−C bond photodissociation has been investigated by time-dependent density functional theory (TD-DFT). At low pH, the MeCbl cofactor adopts the base-off form in which the axial nitrogenous ligand is replaced by a water molecule. Ultrafast excited-state dynamics and photolysis studies have revealed that a new channel for rapid nonradiative decay in base-off MeCbl is opened, which competes with bond dissociation. To explain these experimental findings, the corresponding potential energy surface of the S_1 state was constructed as a function of Co−C and Co−O bond distances, and the manifold of low-lying triplets was plotted as a function of Co−C bond length. In contrast to the base-on form of MeCbl in which two possible photodissociation pathways were identified on the basis of whether the Co−C bond (path A) or axial Co−N bond (path B) elongates first, only path B is active in base-off MeCbl. Specifically, path A is inactive because the energy barrier associated with direct dissociation of the methyl ligand is higher than the barrier of intersection between two different electronic states: a metal-to-ligand charge transfer state (MLCT), and a ligand field state (LF) along the Co−O coordinate of the S_1 PES. Path B initially involves displacement of the water molecule, followed by the formation of an LF-type intermediate, which possesses a very shallow energy minimum with respect to the Co−C coordinate. This LF-type intermediate on path B may result in either S_1/S_0 internal conversion or singlet radical pair generation. In addition, intersystem crossing (ISC) resulting in generation of a triplet radical pair is also feasible.

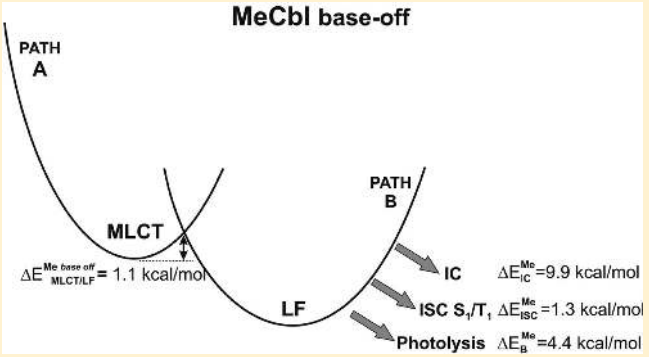

1. INTRODUCTION

Methylcobalamin (MeCbl, Figure 1) is a bioinorganic cofactor[1−3] that belongs to the cobalamins, a class of octahedral Co^{III} complexes containing a planar framework known as corrin, in which the Co metal center is coordinated in the equatorial plane by four nitrogens. The metal center is axially bonded on the lower face by 5,6-dimethylbenzimidazole (DBI), and the upper face by a methyl group.[4,5] The MeCbl cofactor plays a critical role in the number of enzymatic reactions.[6−25] MeCbl-dependent enzymes, known also as methyltransferases,[6−8,10,13−16,18,22,24,25] catalyze the transfer of methyl groups from methyl donors to methyl acceptors. Among these enzymes, cobalamin-dependent methionine synthase (MetH)[13,18,22,24,25] is one of the most well studied, catalyzing the transfer of the methyl group from CH_3−H_4 Folate to homocysteine to form methionine. Other methyltransferases such as CH_3−H_4 Folate:corrinoid-iron/sulfur,[10] a module in the acetyl-CoA sythase enzyme known as methanol:coenzyme M methyl transferase,[6−8,14−16] have also been well studied.

In addition to MeCbl playing an important role as a bioinorganic cofactor, it also displays complex photophysical and photochemical properties.[26−39] These properties have been extensively probed using ultrafast excited-state dynamics, and it was demonstrated that photodissociation of the Co−C bond can be induced by laser light. Experimental studies of the base-on form of MeCbl show that its photolysis depends upon the excitation wavelength.[33,34] Upon excitation at 400 nm, a 25% bond photolysis and subsequent formation of cob(II)alamin and methyl radicals is observed, while the remainder forms a photoproduct with a spectrum similar to that of a cob(III)-alamin intermediate with a weakly attached axial ligand.[33,34] This photoproduct, which is metastable, then undergoes photolysis in about 12%, and the remainder of the population converts to the ground state. Excitation at 520 nm, on the other hand, only produces the metastable intermediate without prompt photolysis[34] and is again partioned between photolysis in about 14%, and conversion to the ground state. The key metastable photoproduct present during both photolysis processes was identified as an S_1 state with metal-to-ligand charge transfer character (MLCT). In strongly acidic conditions

Received: December 3, 2014
Revised: April 1, 2015
Published: April 2, 2015

DOI: 10.1021/jp5120674
J. Phys. Chem. A 2015, 119, 3913−3928

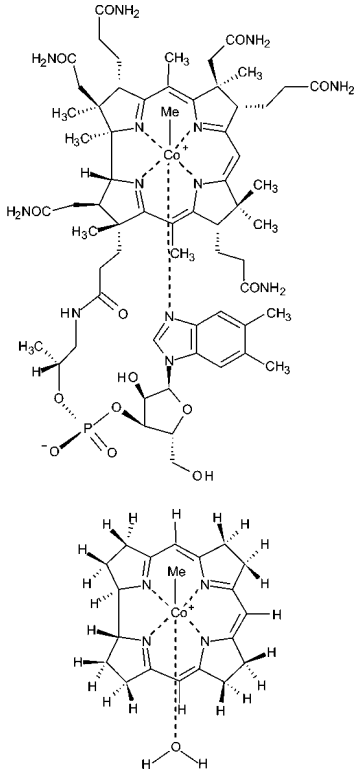

Figure 1. Top: Molecular structure of methylcobalamin (MeCbl). Bottom: Structural model of base-off form of MeCbl employed in the present work.

(pH ≈ 2), the protonated DBI is replaced by water, leading to the formation of MeCbl in its base-off form. Interestingly, the photoproperties of base-off MeCbl are very different from those of the base-on analogue. The absence of the axial nitrogenous DBI ligand in the base-off configuration alters the electronic structure of MeCbl, and opens a channel for fast nonradiative decay, which effectively competes with the channel for Co−C bond photodissociation.[39]

To characterize the mechanism of Co−C bond photodissociation in the base-on form of MeCbl, density functional theory (DFT)[40−43] and time-dependent DFT (TD-DFT)[44−48] were previously used to calculate a low-lying manifold of singlet and triplet excited states as a function of Co−C bond distance.[49,50] Consistent with experimental results,[35,37] the metastable photoproduct was determined to be the S_1 state, which had dominant MLCT character.[49−51] Initially, a repulsive $^3(\sigma_{Co-C} \rightarrow \sigma^*_{Co-C})$ triplet state was proposed to have an influence in bond photolysis,[49,50] because this state drops in energy along the Co−C coordinate, and becomes dissociative for distances longer than 2.4 Å. However, magnetic field effect investigations,[52] and transient absorption studies indicating a prominent geminate recombination component,[38] put the involvement of this triplet radical pair into question, and implied that photolysis should occur via singlet species. Taking into account the aforementioned experimental observations, the mechanism of Co−C bond photolysis in the base-on form of MeCbl was then reinvestigated, and the probability of intersystem crossing involving $S_n/^3(\sigma_{Co-C} \rightarrow \sigma^*_{Co-C})$ was scrutinized.[53] On the basis of Landau−Zener theory, the spin-forbidden crossing between the S_1 and the repulsive triplet state was found to be unlikely as a result of a large gradient difference between these states.[54,55] In addition, the value of spin−orbit coupling in spin-forbidden processes is typically small for transition metals of the first row. It was thus concluded that the triplet state is not involved in base-on MeCbl, and that photolysis should consequently occur through singlet pathways. The potential energy surface (PES) of this S_1 state was constructed as a function of Co−C and Co−N axial bond distances, and two possible photodissociation pathways were identified on the basis of energetic grounds.[53]

The purpose of the present study is to further investigate Co−C bond photodissociation in the base-off form of MeCbl, consistent with the concurrently reported mechanism for base-on MeCbl. TD-DFT was applied to obtain the S_1 PES as a function of Co−C and Co−O axial bond distances, a minimum energy path for Co−C bond cleavage was located on this surface, and a corresponding mechanism was proposed. This mechanism was compared to current experimental data, and both similarities and differences between base-on and base-off forms of MeCbl were analyzed. Although lower cobalamin ligands have been shown to have little influence on the properties of their ground states, as recently reviewed,[56,57] the role of axial base becomes increasingly significant when excited states, and thus mechanisms responsible for photolytic cleavage of cobalamins are considered, as shown by Sension et al.[39] Finally, an explanation is provided showing that the absence of DBI opens a channel for fast nonradiative decay, which effectively competes with Co−C bond photodissociation.

2. COMPUTATIONAL DETAILS

Taking into account that there is no structural data available for base-off MeCbl, the X-ray structure of base-on MeCbl[4] was used and modified. The MeCbl structure was simplified with respect to side chains, and water was assumed as the lower ligand (Figure 1). Throughout this study, the truncated MeCbl model will be referred to as $H_2O-[Co^{III}(corrin)]-Me^+$, which corresponds to an overall charge of +1, and singlet spin multiplicity. To account for the effects of a water solvent on the electronic and molecular structure, ground and electronically excited states were computed with the use of the Conductor-like Screening Model (COSMO).[58,59]

In accordance with previous studies, all DFT[43] and TD-DFT[44,45] calculations reported herein were carried out with the BP86 exchange-correlation functional,[60,61] and triple-ζ quality basis sets as implemented in Turbomole[62] for all atoms, TZVPP for Co, C, N, and TZVP for H.[63] Resolution of Identity for computing the electronic coulomb interaction (RI-J)[64] was applied with respective auxiliary basis sets[65] for RI-DFT. Both geometries and bond dissociation energies (BDEs) for cobalt-containing corrinoids have been successfully predicted at this level of theory.[66−71] In particular, previous benchmarks regarding the S_1 state in base-on MeCbl calculated using BP86 were shown to be consistent with both experiment and wave function-based methods.[51] We have also shown that TD-DFT calculations performed on truncated corrin models produce the best agreement with experiment when GGA (i.e., BP86) instead of hybrid (i.e., B3LYP) exchange-correlation functionals are used,[72] and that the accuracy of calculated excitation energies is more sensitive to functional than basis set. It should be noted that when the full cobalamin structure is considered at the same level of theory, the main difference between the full and truncated systems lies in subtle differences in the character of low-lying electronic transitions, not in their relative energies to the ground state. In other words, as may be expected because of greater electron density most transitions of

DOI: 10.1021/jp5120674
J. Phys. Chem. A 2015, 119, 3913−3928

Table 1. Selected Geometrical Parameters and NBO Charges for $H_2O-[Co^{III}(corrin)]-Me^+$ Model Complex and Other Species Involved in the Photoreaction Process

	geometry		NBO charges				
			$H_2O-[Co^{III}(corrin)]-Me^+$				
	I (S_{0min})	I (S_{1min})		q_{S0} (S_{0min})	q_{S0}[a] (S_{1min})	q_{S1}	Δq[b]
	bond distances [Å]						
Co−C	1.969	1.962	Co	0.765	0.778	0.967	0.189
C−O	2.359	2.217	C	−0.658	−0.673	−0.637	0.036
$Co-N_{21}$	1.876	1.879	O	−0.925	−0.913	−0.895	0.018
$Co-N_{22}$	1.929	1.966	Me	−0.067	−0.083	−0.001	0.082
$Co-N_{23}$	1.928	1.976	H_2O	0.075	0.096	0.125	0.029
$Co-N_{24}$	1.871	1.881	Corr	0.227	0.208	−0.092	−0.300
	bond angles [deg]						
C−Co−O	175.6	164.5					
$N_{21}-Co-N_{23}$	171.2	170.8					
$N_{22}-Co-N_{24}$	173.4	172.7					
			$[Co^{III}(corrin)]-Me^+$				
	IIIB (S_{0min})	IIIB (S_{1min})		q_{S0} (S_{0min})	q_{S0}[a] (S_{1min})	q_{S1}	Δq[b]
	bond distances [Å]						
Co−C	1.968	2.229	Co	0.738	0.777	0.876	0.099
$Co-N_{21}$	1.866	1.857	C	−0.620	−0.617	−0.823	−0.206
$Co-N_{22}$	1.920	1.927	Me	−0.016	−0.013	−0.238	−0.225
$Co-N_{23}$	1.919	1.939	Corr	0.278	0.235	0.362	0.126
$Co-N_{24}$	1.862	1.856					
	bond angles [deg]						
$N_{21}-Co-N_{23}$	167.4	160.4					
$N_{22}-Co-N_{24}$	172.7	173.5					
			$[Co^{II}(corrin)]^+$				
	VIB (S_{0min})	VIB (S_{1min})		q_{S0} (S_{0min})	q_{S0}[a] (S_{1min})	q_{S1}	Δq[b]
	bond distances [Å]						
$Co-N_{21}$	1.875	1.842	Co	0.989	0.983	0.841	−0.142
$Co-N_{22}$	1.926	1.915	Corr	0.011	0.017	0.159	0.142
$Co-N_{23}$	1.926	1.915					
$Co-N_{24}$	1.875	1.843					
	bond angles [deg]						
$N_{21}-Co-N_{23}$	172.0	170.2					
$N_{22}-Co-N_{24}$	172.0	170.2					

[a] q_{S0}: charges in ground state in geometry excited state. [b] Δq: difference between charge in excited state and ground state in geometry excited state.

the full structure contain additional excited-state contributions, and the weights of minor contributions to each state are somewhat higher, but the energies of each transition are essentially unaffected, and as such truncated PESs of cobalamins should be considered accurate.

Initially, the structural model of base-off MeCbl (Figure S1, Supporting Information) was optimized at the DFT/BP86 level of theory using the basis sets described above. Replacement of the axial DBI ligand (that in previous calculations was simplified to imidazole) by water has a rather small impact on the overall structure, with the axial bond length differences being the exception. Comparison of the cobalt−carbon distance in $Im-[Co^{III}(corrin)]-Me^+$ with the analogous distance in $H_2O-[Co^{III}(corrin)]-Me^+$ reveals that the Co−C bond in the former, that is, 1.986 Å (Table 2 and Figure 6 from ref 53), remains almost unchanged in the latter, that is, 1.969 Å. On the other hand, the Co−N axial bond length of 2.175 Å (Table 2 and Figure 6 from ref 53) changes noticeably to 2.359 Å in the case of Co−O. Such a change indicates that water is very weakly coordinated to the Co center in the base-off form of MeCbl (Table 1).

Low-lying electronically excited states of $H_2O-[Co^{III}(corrin)]-Me^+$ and their subsequent optimizations were calculated at the TD-DFT/BP86 level. Vertical excitations were determined with respect to relevant axial bond lengths of the optimized ground state. The corresponding relaxed one-dimensional and two-dimensional potential energy surfaces (PESs) of the S_1 state were then calculated from these points.

The relevant intermediates involved in photolysis were located on the S_1 PES representing the $H_2O-[Co^{III}(corrin)]-Me^+$ system with either a Co−C bond that is weakly or fully broken, or a water molecule that is weakly or fully detached. Whenever possible, optimizations of the relevant S_1 PES intermediates were carried out assuming either a five- or four-coordinate geometry. The key species associated with important points on the photoreaction path were reoptimized using Grimme's empirical dispersive energy correction.[73]

Notation of the base-off MeCbl model consistent with a previous study was used. The subscript X in $\{H_2O-[Co^{III}(corrin)]-Me^+\}_X$ represents the specific state and major electronic configuration. For example, $X = 0$ represents the ground state, whereas $X = 1$,MLCT represents the first excited state with MLCT character. Additionally, intermediates with axial bonds that are elongated or partially ruptured are noted as $\{H_2O-[Co^{III}(corrin)]^+\cdots Me\}_X$, whereas an axial bond that is fully dissociated is noted as $\{H_2O-[Co^{II}(corrin)]^+ + {}^\bullet Me\}_X$.

DOI: 10.1021/jp5120674
J. Phys. Chem. A 2015, 119, 3913−3928

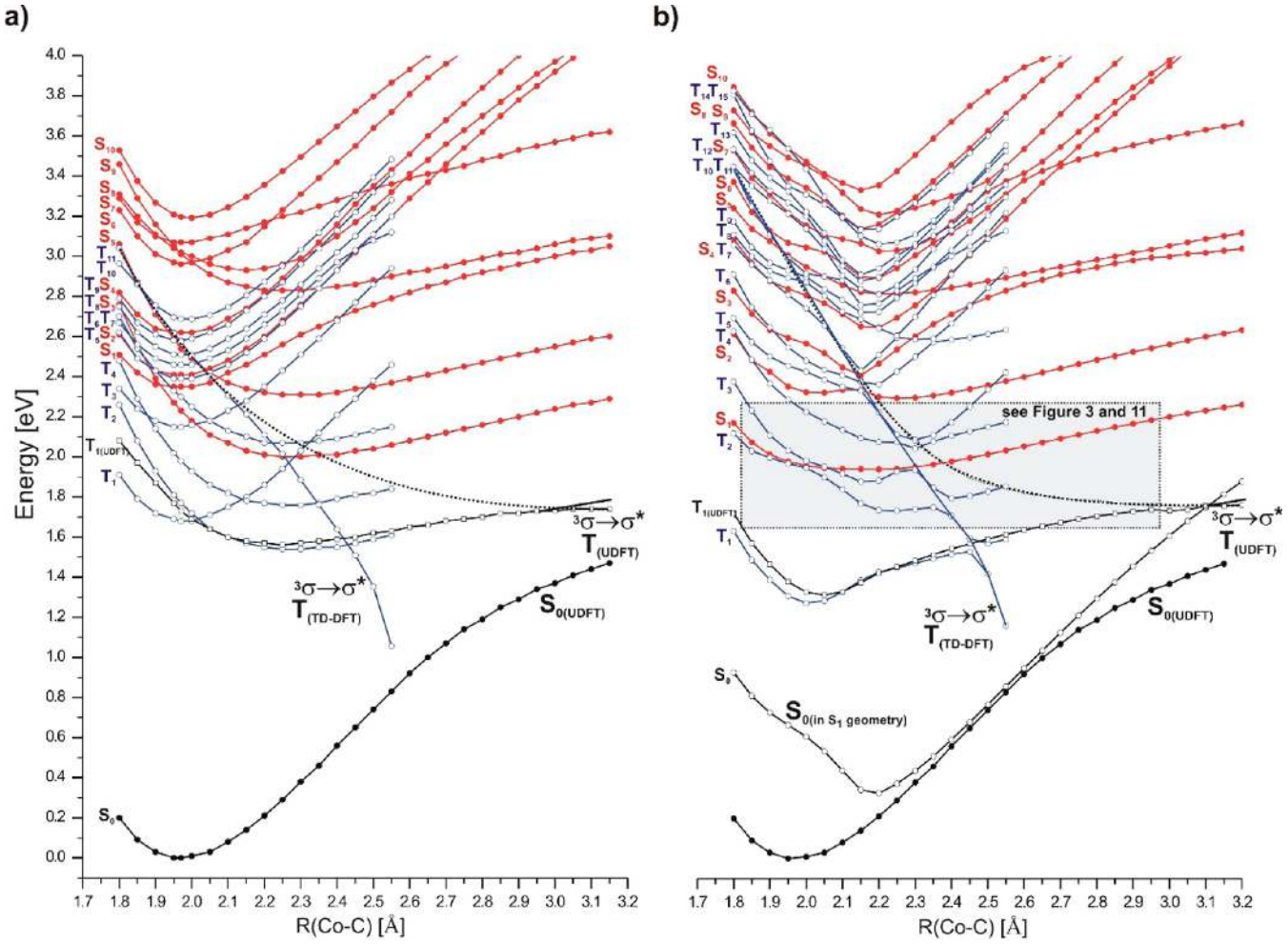

Figure 2. Potential energy curves of the ground and lowest-excited states (singlet and triplet) of the $[Co^{III}(corrin)]-Me^+$ model complex along the Co−C bond stretch computed at the ground-state optimized geometry (a) and at the S_1 state optimized geometry (b). The dotted line corresponds to the approximate course of the triplet excited state $^3(\sigma_{Co-C} \rightarrow \sigma^*_{Co-C})$.

3. RESULTS AND DISCUSSION

3.1. Low-Lying Excited States along Co−C Stretched Coordinate. Consistent with previous studies,[49,50,53] a low-lying excited-state manifold of singlets and triplets was computed along the Co−C coordinate. The five-coordinated $[Co^{III}(corrin)]-Me^+$ species was taken without weakly coordinated water due to the fact that upon excitation there is a tendency for axial ligand displacement. A step size of 0.05 Å was used to systematically elongate the Co−C bond, and the corresponding structures (S_0) were optimized at each point. These geometries were then used to calculate a number of excited singlets and triplets, up to around 3.6 eV to include electronic transitions relevant from a photochemical perspective. The transitions of each excited state were then analyzed, and plotted as a function of corresponding coordinate (Figure 2a).

It is important to point out that vertical excitations were initially calculated without relaxing the corresponding geometries in their excited states. In the case of base-off MeCbl, none of the singlet states were found to have repulsive character. On the other hand, repulsive states within the lower triplet manifold, specifically a $^3(\sigma_{Co-C} \rightarrow \sigma^*_{Co-C})$ state that drops in energy along the Co−C coordinate, were noted at the TD-DFT level. To further verify the repulsive nature of this state, the lowest triplet transition was also calculated using an UDFT framework. Both triplet states are presented in Figure 2a, and labeled $T_{(TD\text{-}DFT)}$ and $T_{(UDFT)}$, respectively. Although these states are composed of the same orbital contributions, as may be expected due to the instability of the single determinant-based wave function at longer Co−C distances, the energy of the TD-DFT state drops faster, while the energy of the $T_{(UDFT)}$ state levels off. $T_{1(UDFT)}$ up to about 3.05 Å has a dominant $d_{yz} \rightarrow \sigma^*$ contribution, whereas at longer distances it changes to $^3(\sigma_{Co-C} \rightarrow \sigma^*_{Co-C})$ as a result of crossing between two different triplet states, although the UDFT procedure allows only the lowest energy state to be obtained. The dotted line in Figure 2a is an interpolation between TD-DFT $^3(\sigma_{Co-C} \rightarrow \sigma^*_{Co-C})$ at short Co−C distances, and the respective UDFT state at long distances, and is the best approximation of the shape of the dissociative triplet state.

A comparison of Figure 2a with the corresponding figure for base-on MeCbl[53] indicates that the absence of the axial base has a relatively small influence on the ground state (S_0). This observation is consistent with experimental results wherein replacement of axial base was shown to have relatively minor influence on the bond dissociation energy (BDE).[74] This is also consistent with resonance Raman spectroscopy studies, wherein it was shown that the stretching vibration of the Co−C bond was insensitive with respect to base-on/-off configuration.[75]

DOI: 10.1021/jp5120674
J. Phys. Chem. A 2015, 119, 3913−3928

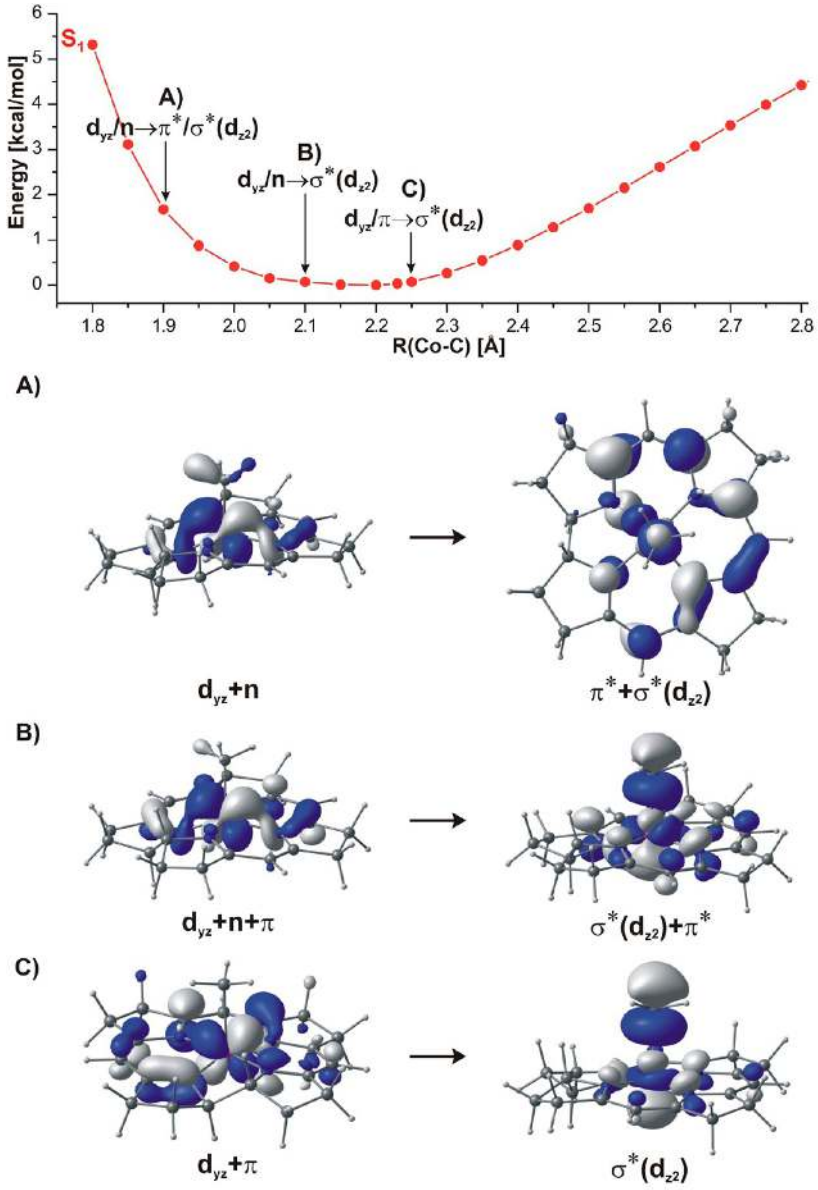

Figure 3. Potential energy curve for S_1 optimized geometry of the $[Co^{III}(corrin)]-Me^+$ model complex along the Co−C bond stretch (upper panel). Molecular orbitals (MOs) describing the S_1 excited state and the character of this state at three various points on the potential energy curve (lower panels).

Taking into account that the vertical excitations were generated from the ground state, and that both ground states are similar, it can be concluded that the manifolds of low-lying singlet excited states have similar character, whereas more differences may be noticed among the triplet excited-state manifolds.

When the S_1 state was optimized along the Co−C coordinate, its energy drops by about 0.06 eV and the potential energy curve corresponding to the S_1 state becomes very shallow. Not much change in energy is observed in the range of 2.0−2.4 Å. Also, a number of triplet states are very close in energy to S_1 states corresponding to the relaxed excited-state geometry. To emphasize the most important region of the excited-state manifold, a box is drawn around singlet and triplet states of the base-off configuration (Figure 2b).

To further understand the nature of the S_1 state, a number of points corresponding to the potential energy curve for the relaxed S_1 state were analyzed in terms of the orbitals involved in excitation (Figure 3). Regarding the Co−C distance of 1.9 Å, the main contribution is from a $d_{yz}/n \rightarrow \pi^*/\sigma^*(d_z^2)$ transition, and is very similar to the vertical excitation (Table S3, Supporting Information). When bond distances increase from 1.90 through 2.25 Å, a change occurs in the character of the excited state that corresponds to a decrease in π^* character, and an increase in σ^* character. In fact after 2.20 Å, the excited electron essentially populates a pure antibonding σ^* orbital. It is interesting to point out that this behavior of the S_1 state is similar to the reductive cleavage mechanism of MeCbl in which the change in electronic energy was associated with the addition of one electron to the ground state.[70]

3.2. Potential Energy Surface of the S_1 State. To obtain a reliable description of the PES associated with the lowest electronically excited states of base-off MeCbl, the optimized structure with water as the axial ligand, represented as $\{H_2O-[Co^{III}(corrin)]-Me^+\}$, was used as an initial starting point. Starting from this geometry, the PES corresponding to S_0 was generated as a function of Co−C and Co−O bond distances by

DOI: 10.1021/jp5120674
J. Phys. Chem. A 2015, 119, 3913−3928

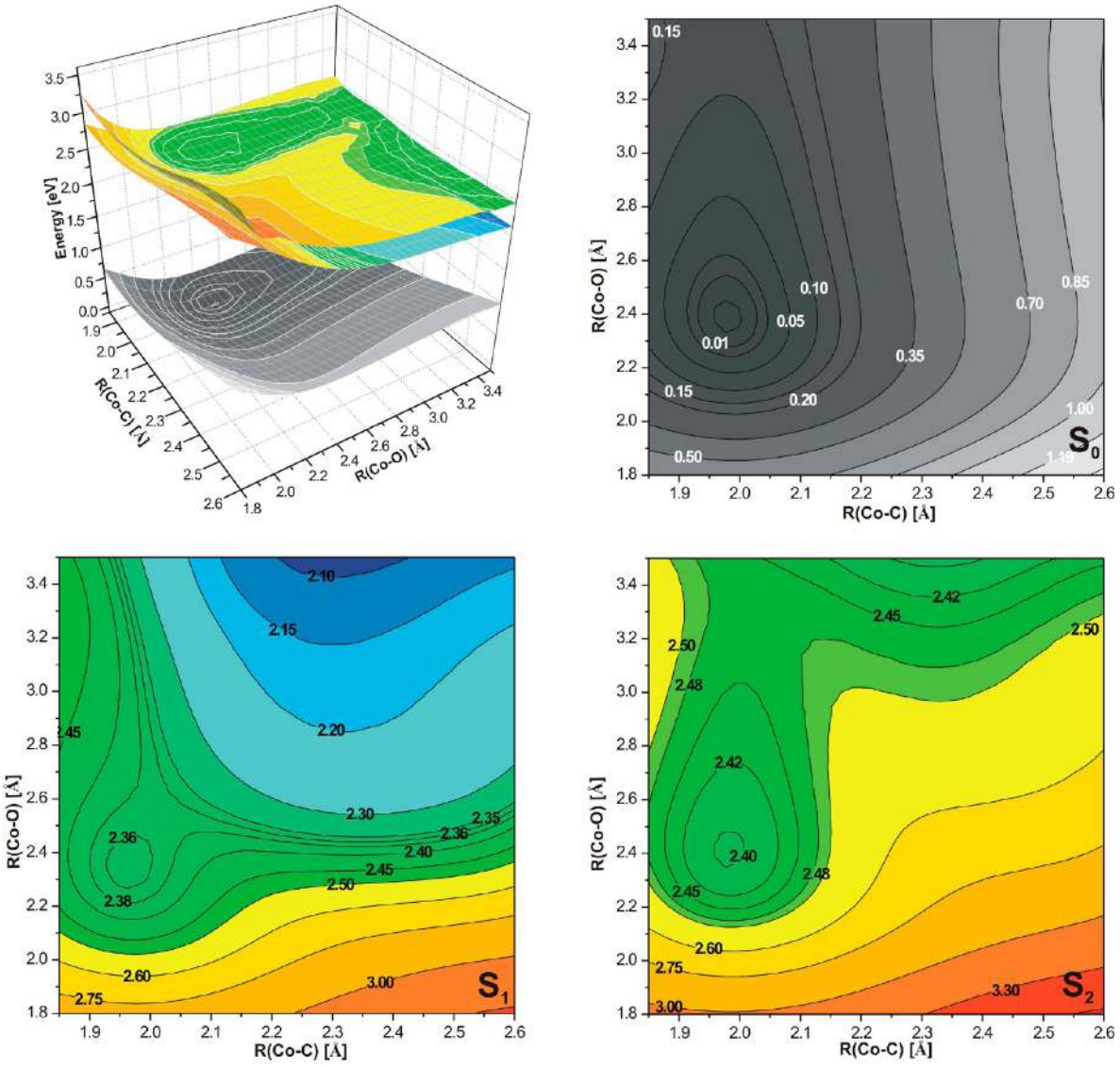

Figure 4. Potential energy surfaces for singlet ground state and the two lowest, singlet excited states of $H_2O-[Co^{III}(corrin)]-Me^+$ together with their vertical projections plotted as a function of axial bond lengths.

systematically elongating each bond with a step size of 0.05 Å, and optimizing all other coordinates (Figure 4, S_0 surface). At each point, vertical excitations were calculated using TD-DFT/BP86. The resulting two-dimensional S_0 PES and corresponding S_1 and S_2 state PESs are shown in Figure 4. The S_0 state minima have a Co−C axial bond length of 1.969 Å and a Co−O axial bond length of 2.359 Å. As mentioned, no crystal structure is available for the base-off form of MeCbl, and thus comparison with structural data cannot be provided. However, the Co−O axial bond length is noticeably longer than the Co−N_{DBI} distance of 2.249 Å calculated at the DFT/BP86/TZVPP level of theory using the similar $\{DBI-[Co^{III}(corrin)]-Me^+\}$ structural model. The Co−N_{DBI} bond length is comparable with the X-ray value of 2.163 Å reported in ref 4.

Overall, the topology of S_0 surface is very shallow, especially along the Co−O direction. The S_1 PES calculated as vertical excitations shows two energy minima, one above the minimum corresponding to the S_0 state, and the second with weakly coordinated axial water and a Co−C bond length of around 2.4 Å. Although the second minimum is much lower in energy, due to the instability of the TD-DFT single-determinant-based wave function at very long bond lengths, this region cannot currently be fully explored. The S_2 PES has a topology similar to that of S_1, and the minimum clearly visible above S_1 is very shallow in the same direction as the lowest minima of the S_1 PES. Similar to base-on MeCbl, although less visible, the PES corresponding to the base-off form of MeCbl also has a seam along the Co−C direction. The presence of this seam will become more apparent when the relaxed S_1 surface is discussed below.

To further characterize the S_1 surface, each point generated as a vertical excitation was optimized. The relaxed S_1 state PES is presented in Figure 5a along with the corresponding relaxed S_1 surface for the base-on analogue. The energy diagram for all species on the S_1 PES is shown in Figure S2 in the Supporting Information. There are two main differences between the vertical and relaxed S_1 PESs (Figures 4 and 5a). There are two minima associated with both vertical and relaxed S_1 PESs. On the relaxed S_1 surface, the first minimum becomes energetically lower than the corresponding minimum on the vertical S_1 PES, and from an energetic point of view is comparable to that of the second minimum. This second minimum on the relaxed S_1 PES

DOI: 10.1021/jp5120674
J. Phys. Chem. A 2015, 119, 3913−3928

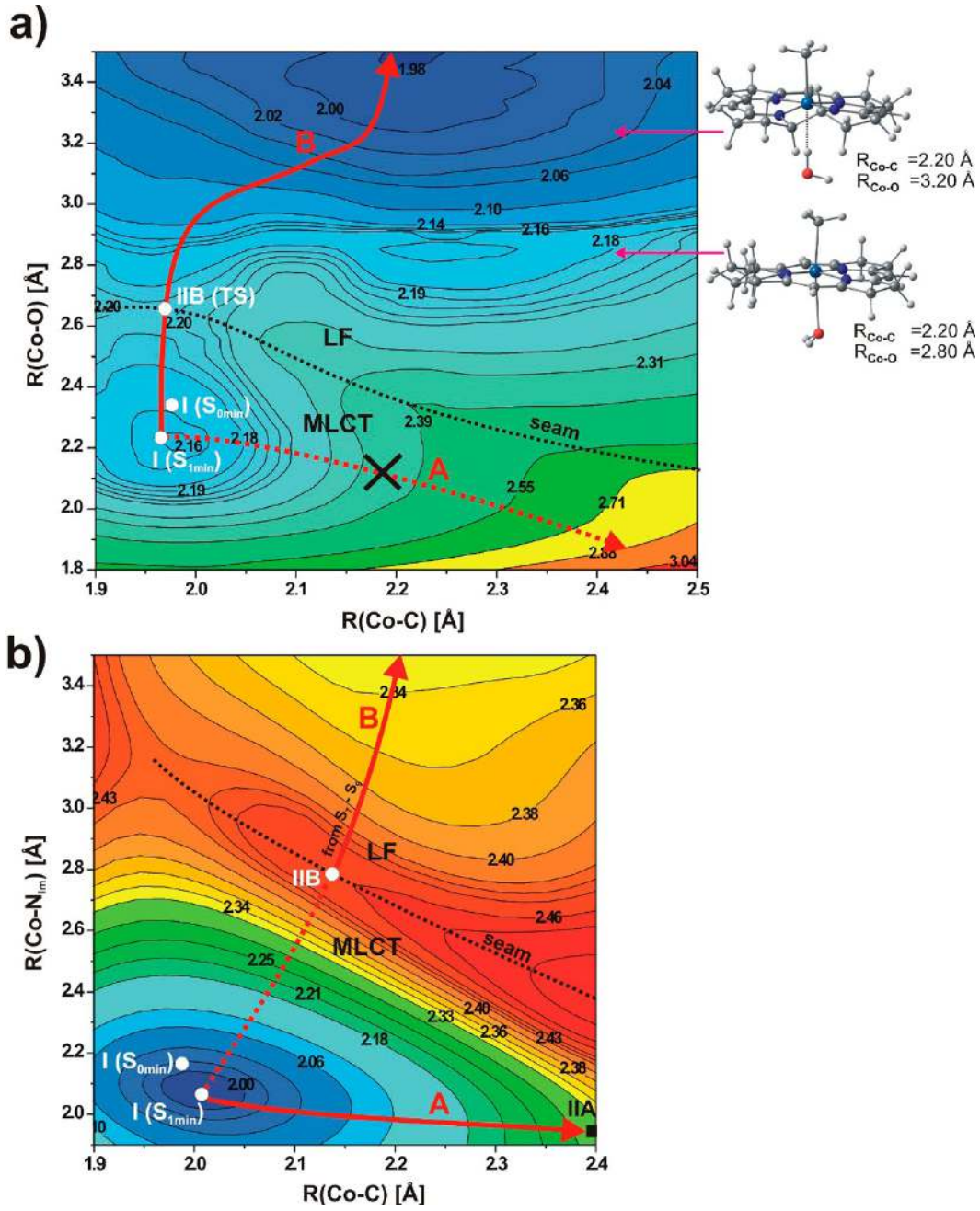

Figure 5. Potential energy surface for the S_1 electronic state in the optimized geometry of the excited state plotted as a function of axial bond length (a) for $H_2O-[Co^{III}(corrin)]-Me^+$ and (b) for $Im-[Co^{III}(corrin)]-Me^+$ model complexes.

becomes very shallow along the Co−C direction, and indeed the seam between these two minima that results in the crossing of two surfaces is now more visible. The area associated with this first minima corresponds to metal-to-ligand charge transfer (MLCT), whereas the other minimum corresponds to a ligand field (LF) transition. A number of intermediates can then be associated with the relaxed S_1 PES as summarized in Table 1 and Figure 6. The first intermediate I (S_{1min}), lies above I (S_{0min}), and is lower in energy than the vertical excitation, has a Co−C bond distance of 1.962 Å, and is comparable to the ground-state bond distance of 1.969 Å. The Co−O bond of I (S_{1min}) is also noticeably shorter (2.217 Å) when compared to the ground state value (2.359 Å). Furthermore, the bond angles associated with the O−Co−C moiety in I (S_{1min}) is more bent, and the extent of bending as compared to the ground state is about 12° (Table 1 and Figure 6). The estimation of the structure associated with the shallow minimum of the relaxed S_1 PES was more challenging due to the tendency of the axial water ligand to be detached. Therefore, the more valid comparison would be between the ground state and a corresponding intermediate without water. Direct comparison of IIIB (S_{1min}) with IIIB (S_{0min}) shows the essential difference as the Co−C bond length, between 2.229 and 1.968 Å, which is about 0.261 Å.

3.3. Reaction Pathway Associated with Co−C Bond Dissociation on the S_1 PES. Having discussed the basic properties, and the nature of the intermediates associated with the S_1 PES, now we may turn our attention to the possible photodissociation pathway of the Co−C bond, shown in Figure 7. Before such discussion is presented for base-off MeCbl, it is

DOI: 10.1021/jp5120674
J. Phys. Chem. A 2015, 119, 3913−3928

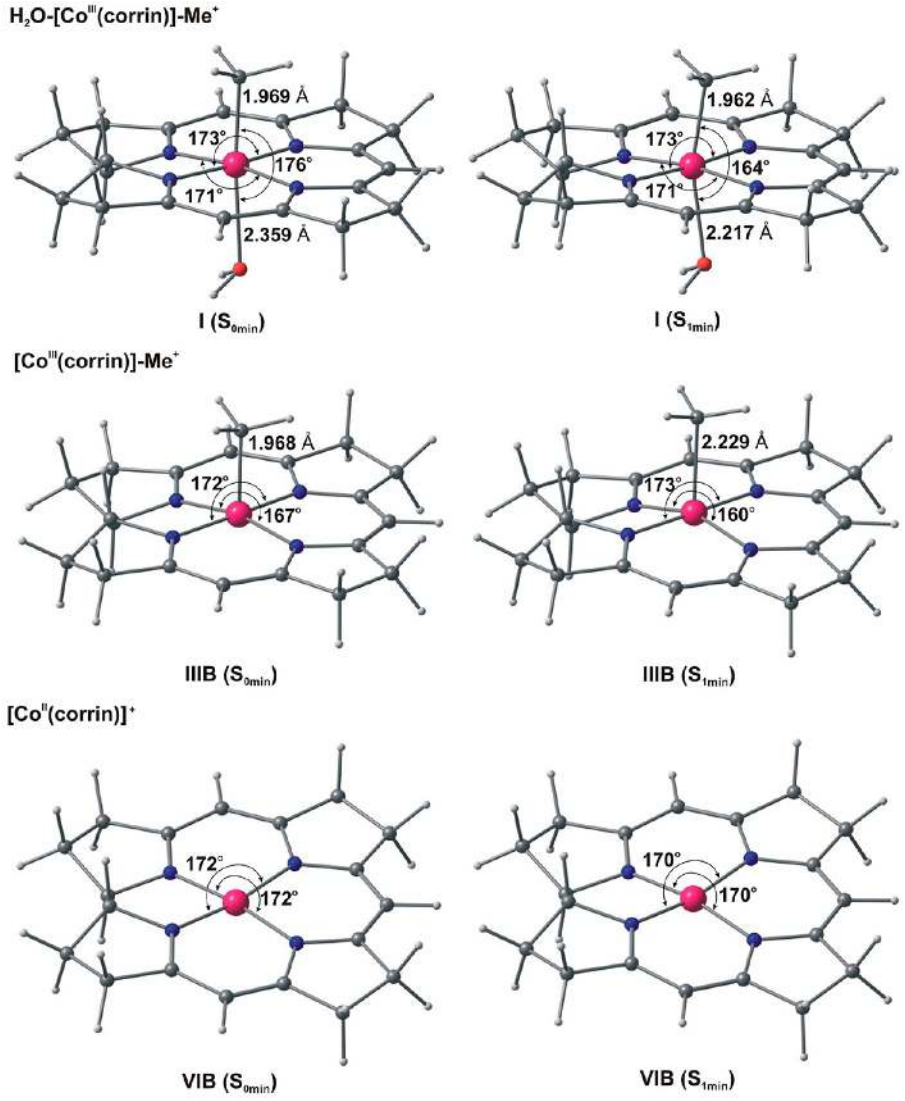

Figure 6. Structures of the most important species on path B from Figures 5 and 7.

relevant to make a short reference to the corresponding S_1 PES of base-on MeCbl (Figure 5b). Comparing the relaxed S_1 surfaces between the base-on/-off forms (Figure 5a and b), the key differences between these two surfaces lie in their topologies with respect to their seams. In the case of base-on MeCbl, the region of the S_1 PES associated with MLCT lies energetically lower than the LF region, implying that the transition from MLCT to LF is an uphill process. On the other hand, for the base-off case, the LF region is now lower than the MLCT, indicating that crossing the seam is energetically accessible. On the basis of energetic grounds, the S_1 state associated with base-on MeCbl has two possible pathways for photodissociation described as path A and path B.[53] Both pathways start from the energy minimum characterized as S_1 MLCT, and proceed along the S_1 PES either through first elongation of the Co−C bond and detachment of the axial base (path A), or first detachment of axial base, followed by elongation of the Co−C bond (path B). Although the starting point and final products are the same for both pathways, the intermediates involved are different.

Similar analysis of the S_1 PES of the base-off form reveals that only one energetic pathway is effective (Figures 5a and 7). This path is labeled as path B, consistent with previous study. The energy diagram for photoreactions on path B is presented in Figure S2 of the Supporting Information, and the schematic drawn on the potential energy curves along Co−O and Co−C bond lengths for electronic states of species involved in photoreaction is shown in Figure 7. As will be described in further detail, path B initially proceeds through detachment of the weakly coordinated axial water. On the other hand, path A initially should proceed through elongation of the Co−C bond and a small contraction of the Co−O bond of the axial water. By analogy with previous work, the initial state is MLCT, and later changes to LF. However, with water attached, the energy along the Co−C distance as can be seen in Figures 5a and 7 increases rapidly. Thus, it can be concluded that path A is inactive in the base-off form of MeCbl on the basis of energetic grounds.

3.4. Photodissociation along Path B Involving a Singlet Radical Pair. The route for Co−C photodissociation starts initially from the S_1 energy minimum labeled I (S_{1min}) (Figures 7 and 8), which has dominant MLCT character. The MLCT nature of this state can be characterized by an electron density shift from the cobalt center of the complex to the corrin

DOI: 10.1021/jp5120674
J. Phys. Chem. A 2015, 119, 3913−3928

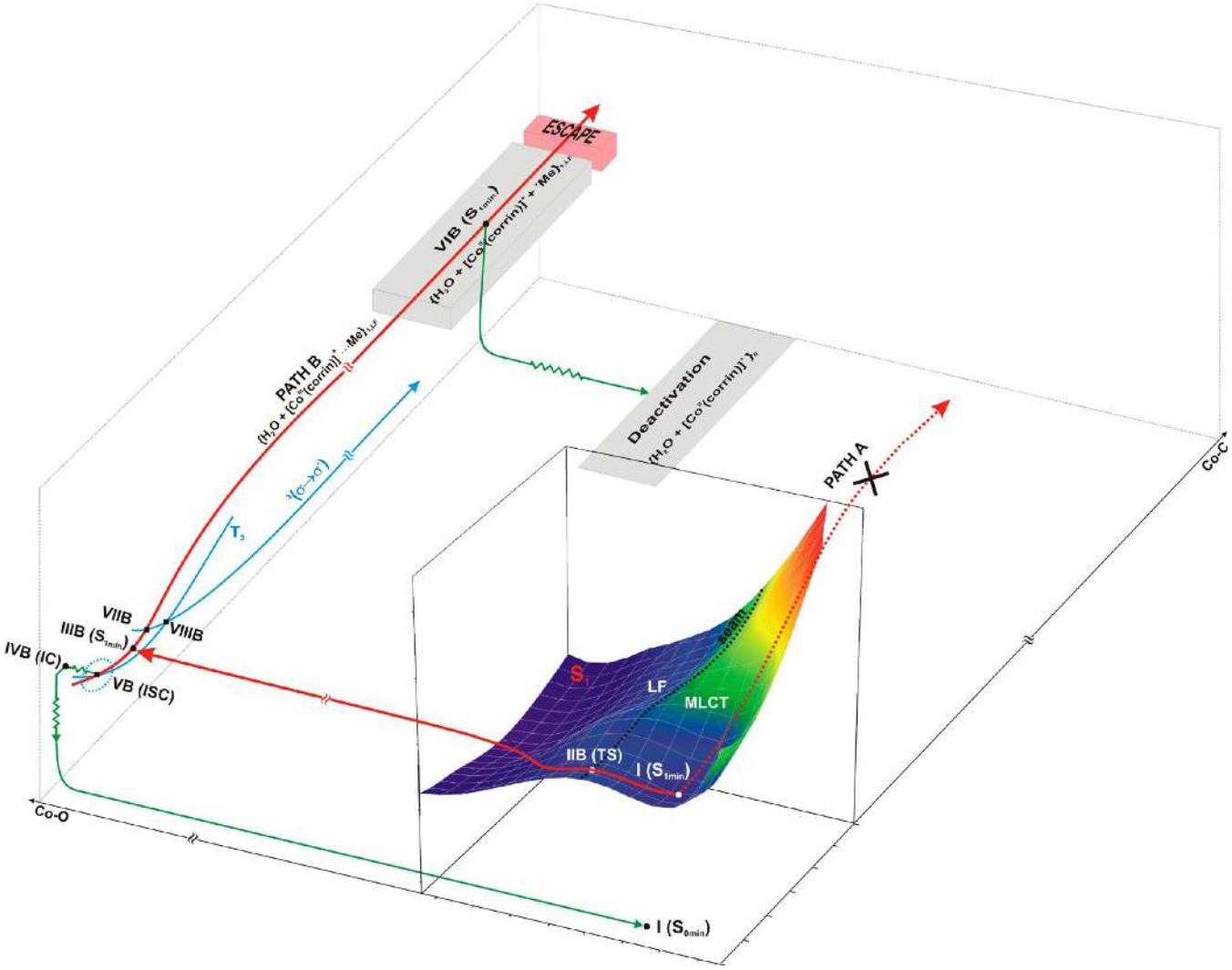

Figure 7. Scheme of photoreaction on path B. Path A is not active for the base-off form of methylcobalamin.

ring, and is discernible on the basis of NBO analysis (Natural Bond Orbital analysis),[76] summarized in Table 1. In addition, the MLCT character of the S_1 state for $H_2O{-}[Co^{III}(corrin)]{-}Me^+$ in I (S_{1min}) is also confirmed by the electron density differences between the S_1 and S_0 states, and is shown in Figure S3 of the Supporting Information. The minimum energy path proceeds in a parallel direction with respect to the Co−O coordinate, and at a Co−O bond length of about 2.65 Å, reaches a transition state, labeled IIB (TS), which can be viewed as occurring on a seam between d → π^* (MLCT) and d → σ^* (LF) states. With increasing Co−O distance, the σ^* orbital gets successively lower in energy, and after reaching the IIB (TS) point it becomes LUMO orbital. The σ^* orbital as LUMO is characteristic for all points on S_1 PES of LF state and other species with detached water ligand on path B (Figure S4, Supporting Information). The small energetic barrier of 1.1 kcal/mol corresponding to the intersection between these two regions of the S_1 PES is about 10 times smaller than the transition state barrier of 10.9 kcal/mol for the similar base-on configuration.[53] Because the transition state IIB (TS) was located by interpolation, the associated numerical values should be taken with some caution. However, the corresponding ratios between transition state energy barriers for base-on and base-off MeCbl should be considered reliable. Once the reaction intermediate passes transition state IIB (TS), the process becomes spontaneous until it reaches the part of the PES labeled IIIB (S_{1min}) (Figures 7 and 8). At this stage water is very weakly attached, that is, $\{H_2O{\cdots}[Co^{III}(corrin)]{-}Me^+\}_{1,LF}$ and resembles a five-coordinate species with no axial base. Interestingly, reorientation of the axial water was observed when the structure reaches IIIB (S_{1min}), indicating increased electron density on Co. This type of interaction resembles the formation of a hydrogen bond, which takes place in the case of Co^I in which the d_{z^2} orbital is doubly occupied.[77] Increasing the electron density on the cobalt atom can also be found on the basis of differences between the $S_{1,LF}$ and S_0 states for five-coordinate $\{[Co^{III}(corrin)]{-}Me^+\}_{1,LF}$ (Figure S3, Supporting Information).

Now, from IIIB (S_{1min}) the dissociation of the Co−C bond may be estimated according to the equation:

$$\{H_2O + [Co^{III}(corrin)]{-}Me^+\}_{1,LF} \rightarrow \{H_2O + [Co^{II}(corrin)]^+ + {}^{\bullet}Me\}_{1,LF} \quad (1)$$

and the resulting energy was found to be 4.4 kcal/mol. The energetic intermediates along path B are presented in Figures 8 and S2 in the Supporting Information. It is also interesting to note that when a similar analysis was performed for base-on

DOI: 10.1021/jp5120674
J. Phys. Chem. A 2015, 119, 3913−3928

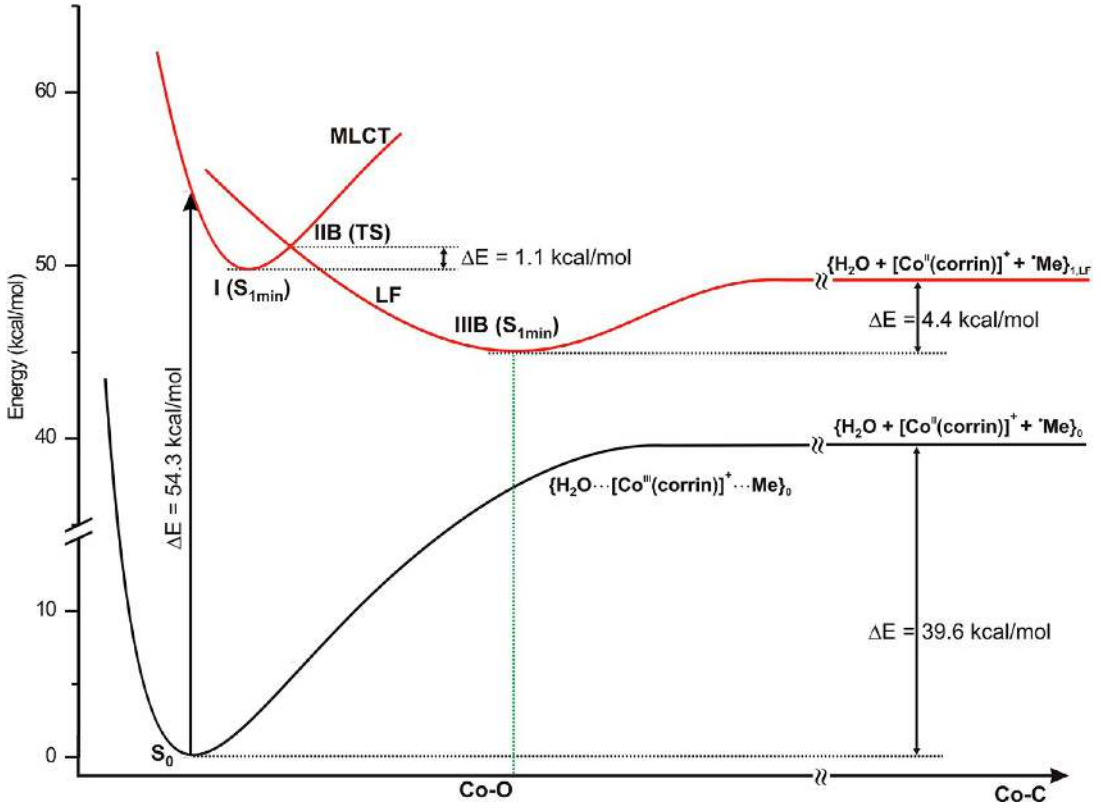

Figure 8. Scheme of potential energy curves along the Co−O and Co−C bond lengths for electronic states of species involved in reaction on path B (the left-hand side in Figure 7).

MeCbl, the corresponding barrier was estimated at 7.9 kcal/mol. The difference related to BDEs is a consequence of the relative energies associated with the points I (S_{1min}), IIB (TS), and IIIB (S_{1min}), between imidazole and water as the axial base. In the S_1 state along path B, when imidazole is present, the energy difference between I (S_{1min}) and IIB (TS) is higher, about 10.9 kcal/mol, and the other point IIIB (S_{1min}) is 3.5 kcal/mol, which is also energetically higher with respect to I (S_{1min}). On the other hand, when water is present as the axial ligand, the energetic relation between points I (S_{1min}) and IIIB (S_{1min}) is reversed. The main difference is that IIIB (S_{1min}) is energetically lower in comparison with I (S_{1min}), demonstrating that the presence of water makes photodissociation through IIIB(S_{1min}) energetically very favorable.

3.5. Internal Conversion along Path B. Along path B, once the system reaches the region IIIB (S_{1min}), which corresponds to a very shallow part of the S_1 PES (Figures 3, 5a, and 7), one can distinguish three possible pathways associated with the electronically excited transient intermediate (Figure 7). The first pathway involves formation of a singlet radical pair that leads to dissociation, as discussed above, the second also leads to dissociation but proceeds through the triplet state as will be discussed further, and the third involves a channel for internal conversion to the ground state.

The mechanism of internal conversion has been discussed in detail in our previous work regarding the base-on form of MeCbl[53] and also involves path B. Because in both cases, the starting point for IC involves a five-coordinated species with detached axial base, it is reasonable to assume that the mechanism of IC in the case of base-off MeCbl proceeds in a similar manner. The important step leading to internal conversion involves distortion of the corrin ring, and can be estimated by the bending angle between the two nitrogen atoms opposite Co, N_{21} and N_{23}. Potential energy surfaces for the S_1 and S_0 states of the $\{[Co^{III}(corrin)]-Me^+\}_{1,LF}$ optimized excited-state geometry as a function of $N_{21}-Co-N_{23}$ valence angle, and Co−C bond length, together with the marked seam along the intersection of the S_1/S_0 are shown in Figure 9a. It has been demonstrated that the active coordinates are the $N_{21}-Co-N_{23}$ valence angle and shortening of the Co−C bond on the S_1 surface, overcoming the S_1/S_0 barrier leading to internal conversion. In the S_1 state of $\{[Co^{III}(corrin)]-Me^+\}_{1,LF}$, shortening the length of the Co−C bond causes a small change in energy, about 0.5 kcal/mol from IIIB (S_{1min}) to 2.00 Å. For an elongated Co−C bond, the $N_{21}-Co-N_{23}$ valence angle changes in the range of 160−143°, without any significant energy barrier. The change of $N_{21}-Co-N_{23}$ valence angle as a function of the Co−C bond length in the S_1 state is presented in Figure 9b. Generally, small changes of the total energy of the S_1 state correspond to changes of these two active coordinates in a relatively wide range of values. These same parameters will significantly increase the ground-state energy, and will ultimately lead to an effective process of IC. It should be noted that the internal conversion process is favorable because it occurs in a wide range of structural configurations. The optimum energy path for IC on the S_1 PES is shown in Figure 9a, and the calculated energy barrier for the S_1/S_0 internal conversion was found to be 9.9 kcal/mol. Nonetheless, the calculated barrier for the S_1/S_0 crossing of 9.9 kcal/mol is likely too large. The main reason for an overestimated IC energy is only two geometrical parameters were considered, and the actual process may involve more active coordinates. The geometry of the intersection point is characterized by a Co−C

DOI: 10.1021/jp5120674
J. Phys. Chem. A 2015, 119, 3913−3928

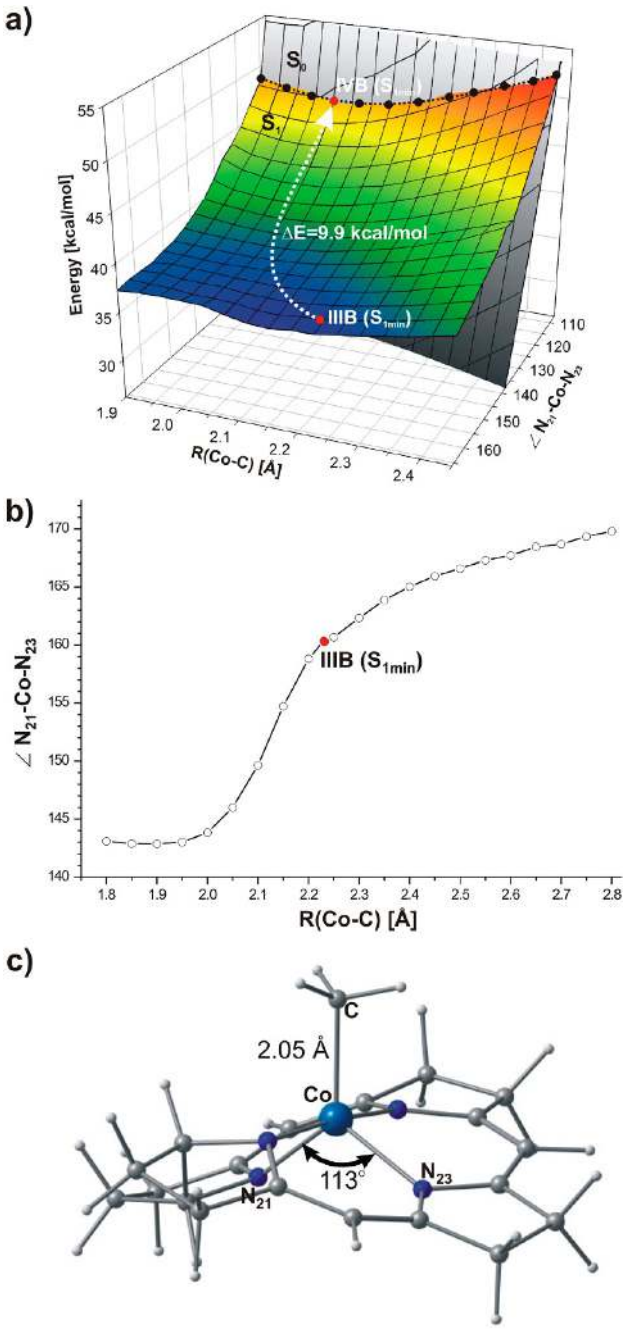

Figure 9. (a) Potential energy surfaces for the S_1 optimized geometry of the $\{[Co^{III}(corrin)]-Me^+\}_{1,LF}$ model complex as a function of $N_{21}-Co-N_{23}$ valence angle and Co−C bond length with the minimum energy path for S_1/S_0 internal conversion depicted. The seam along the intersection of the S_1/S_0 PESs is marked with a dotted black line. (b) $N_{21}-Co-N_{23}$ valence angle as function Co−C bond length in the LF electronic state of $\{[Co^{III}(corrin)]-Me^+\}_{1,LF}$ model complex. (c) Geometry of $\{[Co^{III}(corrin)]-Me^+\}_{1,LF}$ complex at the point of internal conversion.

bond of 2.05 Å and a $N_{21}-Co-N_{23}$ angle of 113°, as shown in Figure 9c.

3.6. Photodissociation versus Internal Conversion: The Importance of Dispersion Corrections. Energetic considerations presented in the two previous sections indicate that photodissociation of Co−C bond along path B should to be more effective than internal conversion. While the calculated barrier for the S_1/S_0 crossing is likely too large, it has been also demonstrated that to obtain reliable Co−C bond dissociation energies dispersion corrections are important.[78,79] Thus, we have recalculated the energies of key intermediates associated with the important points on the potential energy surface to include dispersion, and have summarized them in Figure 10.

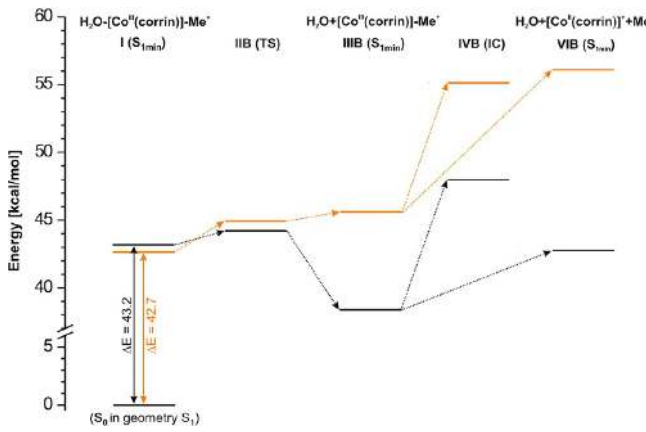

Figure 10. Energy diagram for the most important photoreaction steps along path B (ΔE in kcal/mol): black lines, calculations at the DFT/BP86/TZVPP level of theory; orange lines, calculations with the same method with the use of Grimme's empirical dispersive energy correction.

As expected, the energetic relations on the S_1 potential energy surface do not change significantly when dispersion corrections are added. This is not unexpected, because the states under consideration do not differ substantially in terms of compactness of their ligands. The energetic barriers associated with IVB (IC) and the dissociated VIB (S_{1min}) are now comparable (Figure 10, the last two energy levels marked orange). Although this is an intuitively better outcome because internal conversion and dissociation may now effectively compete, the energy of point IIIB (S_{1min}) with dispersion corrected is somehow a little too high, that is, 0.7 kcal/mol higher than the barrier associated with IIB (TS). Energies for the selected points associated with the LF state near the energy minimum on the PES were also considered (i.e., for R(Co−C) = 2.20 Å and R(Co−O) = 3.20 and 3.50 Å, respectively), and although their values were closer to the energy of I (S_{1min}), they were still lower than the energy of IIB (TS). Taking into account that computed energies relative to dispersion corrections are accurate, and the fact that electronically excited states are being considered, the dissociation energy of water from I (S_{1min}) to IIIB (S_{1min}) is most likely overestimated when dispersion is corrected. In other words, the energy contribution resulting from interactions between water and cobalt in I (S_{1min}) is not adequately compensated for after separation into IIIB (S_{1min}) and H_2O fragments. Our results indicate that elongation of the Co−OH_2 distance should lead to an energy minimum, which is justified considering that negative values for corrections from $[Co^{III}(corrin)]-Me^+$ and H_2O fragments vanish when they are separated. Additionally, the density distribution associated with the S_1 electronic state, characterized by increased density on the cobalt d_{z^2} orbital, is also not properly taken into account. It is therefore reasonable to postulate that the density distribution resulting from an electronically excited state would have a more pronounced energetic effect on IIIB (S_{1min}). Finally, it needs to be pointed out that while the presence of the Co−OH_2 bond is justified, its

DOI: 10.1021/jp5120674
J. Phys. Chem. A 2015, 119, 3913−3928

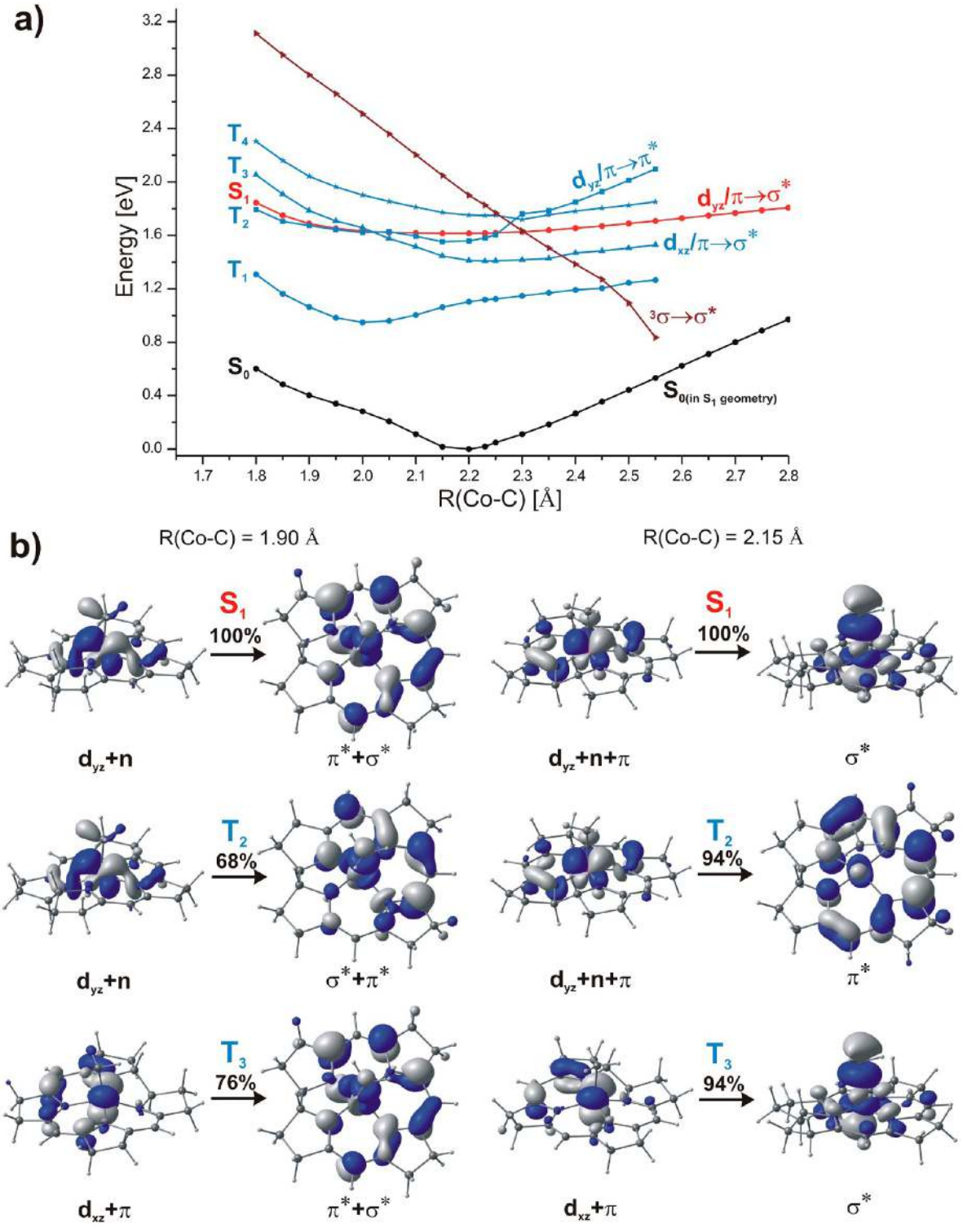

Figure 11. (a) Potential energy curves of the ground (S_0) and selected lowest-excited states (singlet, S_1; and triplets, T_1, T_2, T_3, T_4, and $^3(\sigma_{Co-C} \rightarrow \sigma^*_{Co-C})$) of the $[Co^{III}(corrin)]-Me^+$ model complex along the Co−C bond stretch computed at the optimized geometry of the S_1 state. (b) Molecular orbitals (MOs) describing the singlet and triplet excited states and their character for two different Co−C distances, before and after points of S_1/T_2 and S_1/T_3 intersystem crossing.

formation should have no significant influence on the photoreactions along path B and IIIB (S_{1min}).

3.7. Photodissociation along Path B Involving Intersystem Crossing and Triplet Radical Pair. Parallel to photodissociation from a singlet radical pair along path B, it is also possible that a radical pair may be generated from the triplet state. For dissociation to occur from the triplet state, conversion of a singlet to triplet via intersystem crossing (ISC) must take place. According to Landau−Zener theory,[54,55] a nonzero matrix element involving spin−orbit coupling (SOC) is required, and a small difference in slope should be present between the potential energy curves involved, for an effective

DOI: 10.1021/jp5120674
J. Phys. Chem. A 2015, 119, 3913−3928

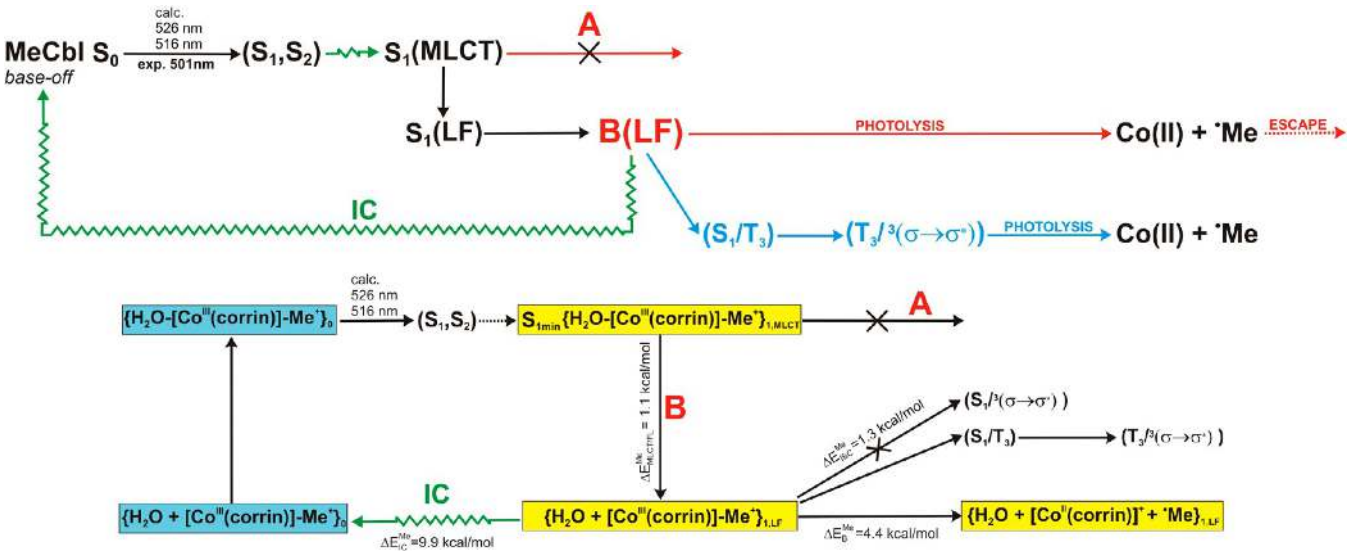

Figure 12. Upper panel: Mechanistic scheme for the photoreaction of the base-off form of MeCbl. Lower panel: Energetics of selected steps of the photoreaction.

crossing of states with different spin multiplicities. Because of the complexity of the base-off form of MeCbl, a good estimation of the extent of SOC is difficult to provide, and would require the use of a multireference wave function. However, on the basis of the potential energy curves shown in Figure 11, the nature of crossing can be readily assessed. Inspection of Figure 11a reveals that states S_1, T_2, and T_3 are very close in energy because they involve the same types of orbitals involved in excitation, and are also nearly parallel to each other over the range of Co−C distances near the energy minimum. On the other hand, T_1 does not interact with S_1, and at a Co−C distance of 2.3 Å a repulsive triplet state, that is, $^3(\sigma \rightarrow \sigma^*)$, crosses with S_1 at a larger angle than T_2 and T_3. When the gradient between diabatic surfaces is small with respect to the minimum-energy crossing point (MECP), the probability of spin-forbidden crossing significantly increases.[80] Thus, it is reasonable to assume that T_2 or T_3 are likely candidates for ISC that occurs from the shallow S_1 surface IIIB (S_{1min}). In addition, according to El-Sayed rules,[81,82] the rate of ISC is relatively large if the radiationless transition involves a change of orbital type. El-Sayed rules have been frequently used to discuss organic molecules in which the typical case is the transition from the lowest excited singlet state to the triplet manifold.[83] For example, the rules predict that ISC involving a $^1(\pi,\pi^*) \rightsquigarrow {}^3(n,\pi^*)$ transition should be faster than a $^1(\pi,\pi^*) \rightsquigarrow {}^3(\pi,\pi^*)$ or a $^1(n,\pi^*) \rightsquigarrow {}^3(\pi,\pi^*)$, and should be faster than a $^1(n,\pi^*) \rightsquigarrow {}^3(n,\pi^*)$ transition. These examples point out that the orbitals involved in a singlet−triplet transition should be rotated 90°.

If one considers a similar analysis involving complexes containing transition metals, electron density redistribution from singlet to triplet should also involve a rotation of the d orbital by 90°, as demonstrated by Zalis et al.[84] A closer inspection of the energy curves and orbitals corresponding to Co−C bond distances of 1.9 and 2.15 Å representing before and after the crossing of S_1 with either T_2 or T_3 (Figure 11) indicates which triplet state should mediate the ISC. When S_1 excitation is considered, the initial transition of $d_{yz} + n \rightarrow \pi^* + \sigma^*$ changes to $d_{yz} + n + \pi \rightarrow \sigma^*$. When the T_2 state is considered, the nature of d orbital character is retained, and the antibonding orbitals involved in the transition change from σ^* to π. On the other hand, the nature of d orbitals of the T_3 excitation changes, whereas the antibonding orbitals remain the same, and essentially are very similar to S_1. Taking the z axis as perpendicular to the corrin plane, the T_2 d_{yz} orbital is rotated by 90° in the T_3 d_{xz} orbital. For the S_1, the d_{yz} orbital is the same as the T_2 d_{yz} orbital, as described above. For S_1 and T_3, the ISC process occurs between the $^1(d_{yz},\sigma^*) \rightsquigarrow {}^3(d_{xz},\sigma^*)$ excited electronic configurations, and it should be concluded that according to El-Sayed rules the SOC rate is enhanced between S_1 and T_3. Taking the above into consideration, the photodissociation mechanism of base-off MeCbl initially involves an intersystem crossing between S_1 and T_3, then T_3 crosses with a repulsive $^3(\sigma \rightarrow \sigma^*)$ triplet state that leads to dissociation, and formation of a triplet radical pair (Figure 11a and points VB (ISC) and VIIIB in Figure 7). This mechanism is similar to our initial proposal, with the exception that an additional triplet (T_3) mediates the transition to the repulsive $^3(\sigma \rightarrow \sigma^*)$ state responsible for Co−C dissociation.

3.8. Implications for the Photochemistry of Base-Off MeCbl. Combining the discussion presented above regarding the nature of the PES associated with the S_1 state, a more general picture of the photochemistry associated with the base-off form of MeCbl may be presented (Figures 12 and 7). On the basis of energetic grounds, in base-off MeCbl the photodissociation channel that initially proceeds along the MLCT surface, referred to as path A, becomes inactive. This is in clear contrast with the base-on form of MeCbl, in which both pathways are considered comparable. The strong preference toward path B is in fact consistent with ultrafast excited-state dynamics of base-off MeCbl. The absence of the trans-nitrogeneous ligand changes the topology of the S_1 state in such a way that the seam between the LF and MLCT regions is significantly shifted toward the minimum, I (S_{1min}), enhancing the LF character of the S_1 state in comparison with that of the MLCT. Within the region of the S_1 PES of base-on MeCbl that can be explored by TD-DFT, the energy minimum is associated with MLCT, whereas in the base-off form it is shifted toward LF. The strong preference for accessibility of the LF state in base-off MeCbl is in agreement with excited-state dynamics

DOI: 10.1021/jp5120674
J. Phys. Chem. A 2015, 119, 3913−3928

studies in which such preference was referred to as opening of a channel for internal conversion, and Co−C bond scission.[39]

Once the system is in the LF minimum, which is energetically very shallow, three different processes compete with each other: photodissociation through the singlet, a similar dissociation involving a triplet that initially proceeds through intersystem crossing, and internal conversion. On the basis of our current calculations and existing experimental data,[39] although IC and bond-homolysis compete, one cannot qualitatively distinguish which photodissociation pathway, singlet or triplet, is more prominent. The absence of a prominent geminate recombination component implies that dissociation through the triplet channel is dominant. This hypothesis may be further proved by application of magnetic field techniques to study the base-off form, and to our best knowledge, to date has only been performed for base-on MeCbl.[52] In sum, it is reasonable to conclude that IC only competes with dissociation via the triplet channel.

It is also interesting to consider the quantum yields reported for the base-on and base-off forms of MeCbl. In the case of base-on, the yield of photodissociation from the excited state is about 0.15,[34] whereas the remaining yields are either IC or recombination. On the other hand, in base-off MeCbl, the dissociation yield from the excited state is 0.65 (+0.15, −0.25),[39] with an error that reflects uncertainties in experimental measurements. The small yield observed in the case of base-on MeCbl, in which photodissociation proceeds via singlet channel, reflects competition with fast deactivation and possible recombination. The much larger quantum yield observed for the base-off form reflects involvement of the triplet state, because once the system converts from S_1 to T_3, and then proceeds via $^3(\sigma \rightarrow \sigma^*)$, there is no possibility for recombination.

4. SUMMARY AND CONCLUSIONS

This work should be considered as a follow-up of our recent theoretical study involving the photochemistry of the base-on form of MeCbl.[53] The aim of the present investigation was to present a mechanism of the base-off form that is in accord with our previous work and current experimental data from ultrafast excited-state dynamics.[34,35,38,39] The present contribution also reconciles our previous model in which involvement of a repulsive triplet state[49,50] was implied. In particular, it has been shown that for effective dissociation to occur from a repulsive triplet state, an additional triplet state should be invoked in accordance with Landau−Zener theory, and according to El-Sayed rules, the SOC matrix elements should contain Co d orbitals from singlet and triplet states rotated by 90°.

The nature of the S_1 state calculated as a function of both axial ligands can be used to elucidate the differences in base-on and base-off forms of MeCbl. The main difference between these two forms can be attributed to a difference in the topology of the S_1 PES and how MLCT and LF states interact with each other. Although in the base-on form, two energetic pathways are feasible, previously described as paths A and B, in the base-off form only path B is effective for photodissociation, and path A is inactive. Possible internal conversion and photodissociation from the triplet state along path B are in accord with current experiment, showing that the absence of DBI opens a channel for fast nonradiative decay, and effectively competes with Co−C bond photodissociation. Further theoretical studies that consider cobalamins with different axial ligands would provide a deeper understanding of the photophysical and photochemical properties of base-off MeCbl.

■ ASSOCIATED CONTENT

Supporting Information

(i) The 10 lowest, vertical singlet and triplet electronic transitions for the $H_2O-[Co^{III}(corrin)]-Me^+$ model complex based on the TD-DFT calculations, (ii) the 10 lowest, vertical electronic transitions for singlets and triplets of the $[Co^{III}(corrin)]-Me^+$ model complex at the TD-DFT level, (iii) the 10 lowest, vertical electronic transitions of the $[Co^{II}(corrin)]^+$ model at the TD-DFT level, (iv) the structural model of base-off MeCbl used herein, (v) the energy diagram of photoreactions on path B, (vi) the HOMO and LUMO molecular orbitals of electronic transitions of the optimized of S_1 states shown with isosurface, and cross-section contours along the axial bond (in two separate planes) of electron density differences between the S_1 and S_0 states for relevant intermediates involved in the photolysis process, and (vii) molecular orbital diagram for species at selected points on path B. This material is available free of charge via the Internet at http://pubs.acs.org.

■ AUTHOR INFORMATION

Corresponding Author

*Phone: (502) 852-6609. Fax: (502) 852-8149. E-mail: pawel@louisville.edu.

Notes

The authors declare no competing financial interest.

■ ACKNOWLEDGMENTS

This work was supported by the National Science Centre, Poland, under grant no. UMO-2013/09/B/ST4/03014. Calculations performed using TURBOMOLE were carried out in the Wroclaw Centre for Networking and Supercomputing, WCSS, Wroclaw, Poland, http://www.wcss.wroc.pl, under calculational grant no. 18, and additionally in the Academic Computer Centre CYFRONET at the University of Science and Technology in Cracow, ACC CYFRONET AGH, Kraków, Poland, http://www.cyfronet.krakow.pl, under grants MNiSW/SGI3700/USląski/111/2007 and MNiSW/IBM_BC_HS21/USląski/111/2007. In addition, we would like to acknowledge the Cardinal Research Cluster (CRC) at the University of Louisville for ensuring computational resources.

■ REFERENCES

(1) *B_{12}*; Dolphin, D., Ed.; John Wiley & Sons: New York, 1982.
(2) *Vitamin B_{12} and B_{12} Proteins*; Kräutler, B., Arigoni, D., Golding, B. T., Eds.; Wiley-VCH: New York, 1998.
(3) *Chemistry and Biochemistry of B_{12}*; Banerjee, R., Ed.; John Wiley & Sons: New York, 1999.
(4) Randaccio, L.; Furlan, M.; Geremia, S.; Slouf, M.; Srnova, I.; Toffoli, D. Similarities and Differences between Cobalamins and Cobaloximes. Accurate Structural Determination of Methylcobalamin and of LiCl- and KCl-Containing Cyanocobalamins by Synchrotron Radiation. *Inorg. Chem.* **2000**, *39*, 3403−3413.
(5) Randaccio, L.; Geremia, S.; Nardin, G.; Wuerges, J. X-ray structural chemistry of cobalamins. *Coord. Chem. Rev.* **2006**, *250*, 1332−1350.
(6) S Shapiro, S.; Wolfe, R. S. Methyl-Coenzyme M, an Intermediate in Methanogenic Dissimilation of C_1 Compounds by Methanosarcina barkeri. *J. Bacteriol.* **1980**, *141*, 728−734.
(7) van der Meijden, P.; Heythuysen, H. J.; Pouwels, A.; Houwen, F.; van der Drift, Ch.; Vogels, G. D. Methyltransferases Involved in

DOI: 10.1021/jp5120674
J. Phys. Chem. A 2015, 119, 3913−3928

Methanol Conversion by Methanosarcina barkeri. *Arch. Microbiol.* **1983**, *134*, 238−242.
(8) van der Meijden, P.; te Brömmelstroet, B. W.; Poirot, Ch. M.; van der Drift, Ch.; Vogels, G. D. Purification and Properties of Methanol:5-Hydroxybenzimidazolylcobamide Methyltransferase from Methanosarcina barkeri. *J. Bacteriol.* **1984**, *160*, 629−635.
(9) Halpern, J. Mechanisms of coenzyme B_{12}-dependent rearrangements. *Science* **1985**, *227*, 869−875.
(10) Ragsdale, S. W.; Wood, H. G. Acetate Biosynthesis by Acetogenic Bacteria. Evidence that carbon monoxide dehydrogenase is the condensing enzyme that catalyzes the final steps of the synthesis. *J. Biol. Chem.* **1985**, *260*, 3970−3977.
(11) Banerjee, R. The Yin-Yang of cobalamin biochemistry. *Chem. Biol.* **1997**, *4*, 175−186.
(12) Ludwig, M. L.; Matthews, R. G. Structure-based perspectives on B_{12}-dependent enzymes. *Annu. Rev. Biochem.* **1997**, *66*, 269−313.
(13) Goulding, C. W.; Postigo, D.; Matthews, R. G. Cobalamin-Dependent Methionine Synthase Is a Modular Protein with Distinct Regions for Binding Homocysteine, Methyltetrahydrofolate, Cobalamin, and Adenosylmethionine. *Biochemistry* **1997**, *36*, 8082−8091.
(14) Sauer, K.; Harms, U.; Thauer, R. K. Methanol:coenzyme M methyltransferase from Methanosarcina barkeri. Purification, properties and encoding genes of the corrinoid protein MT1. *Eur. J. Biochem.* **1997**, *243*, 670−677.
(15) Sauer, K.; Thauer, R. K. Methanol:coenzyme M methyltransferase from Methanosarcina barkeri. Identification of the active-site histidine in the corrinoid-harboring subunit MtaC by site-directed mutagenesis. *Eur. J. Biochem.* **1998**, *253*, 698−705.
(16) Sauer, K.; Thauer, R. K. Methanol:coenzyme M methyltransferase from Methanosarcina barkeri - substitution of the corrinoid harbouring subunit MtaC by free cob(I)alamin. *Eur. J. Biochem.* **1999**, *261*, 674−681.
(17) Marzilli, L. G. The Two B_{12} Cofactors: Influence of the trans Nitrogen Ligand on Homolytic and Heterolytic Processes. In *Bioinorganic Catalysis*; Reedijk, J., Bouwman, E., Eds.; Marcel Dekker Inc.: New York, 1999; pp 423−468.
(18) Matthews, R. G. Cobalamin-Dependent Methyltransferases. *Acc. Chem. Res.* **2001**, *34*, 681−689.
(19) Banerjee, R.; Ragsdale, S. W. The many faces of vitamin B_{12}: catalysis by cobalamin-dependent enzymes. *Annu. Rev. Biochem.* **2003**, *72*, 209−247.
(20) Brown, K. L. Chemistry and Enzymology of Vitamin B_{12}. *Chem. Rev.* **2005**, *105*, 2075−2149.
(21) Hagemeier, C. H.; Kruer, M.; Thauer, R. K.; Warkentin, E.; Ermler, U. Insight into the mechanism of biological methanol activation based on the crystal structure of the methanol-cobalamin methyltransferase complex. *Proc. Natl. Acad. Sci. U.S.A.* **2006**, *103*, 18917−18922.
(22) Matthews, R. G.; Koutmos, M.; Datta, S. Cobalamin-dependent and cobamide-dependent Methyltransferases. *Curr. Opin. Struct. Biol.* **2008**, *18*, 658−666.
(23) Wuerges, J.; Randaccio, L.; Demitri, N.; Geremia, S. Structural aspects of B_{12} chemistry and biochemistry: From simple models to proteins. *Trends Inorg. Chem.* **2009**, *11*, 1−19.
(24) Matthews, R. G. Cobalamin- and Corrinoid-Dependent Enzymes. In *Metal Ions in Life Sciences*; Sigel, A., Sigel, H., Sigel, R. K. O., Eds.; Royal Society of Chemistry: Cambridge, UK, 2009; Vol. *6*, pp 53−114.
(25) Randaccio, L.; Geremia, S.; Demitri, N.; Wuerges, J. Vitamin B_{12}: Unique Metalorganic Compounds and the Most Complex Vitamins. *Molecules* **2010**, *15*, 3228−3259.
(26) Endicott, J. F.; Ferraudi, G. J. A Flash Photolytic Investigation of Low Energy Homolytic Processes in Methylcobalamin. *J. Am. Chem. Soc.* **1977**, *99*, 243−245.
(27) Endicott, J. F.; Netzel, T. L. Early Events and Transient Chemistry in the Photohomolysis of Alkylcobalamins. *J. Am. Chem. Soc.* **1979**, *101*, 4000−4002.
(28) Sakaguchi, Y.; Hayashi, H.; I'Haya, Y. J. Fast Formation of Methyl Radical from Methylaquocobaloxime As Studied by Time-Resolved Optical and ESR Techniques. *J. Phys. Chem.* **1990**, *94*, 291−293.
(29) Chen, E.; Chance, M. R. Continuous-Wave Quantum Yields of Various Cobalamins Are Influenced by Competition between Geminate Recombination and Cage Escape. *Biochemistry* **1993**, *32*, 1480−1487.
(30) Grissom, C. B.; Chagovetz, A. M. Magnetic Field Effects in Model B_{12} Enzymatic Reactions. The Photolysis of Methylcob(III)-alamin. *Z. Phys. Chem.* **1993**, *182*, 181−188.
(31) Lott, W. B.; Chagovetz, A. M.; Grissom, C. B. Alkyl Radical Geometry Controls Geminate Cage Recombination in Alkylcobalamins. *J. Am. Chem. Soc.* **1995**, *117*, 12194−12201.
(32) Natarajan, E.; Grissom, C. B. The Origin of Magnetic Field Dependent Recombination in Alkylcobalamin Radical Pairs. *Photochem. Photobiol.* **1996**, *64*, 286−295.
(33) Walker, L. A., II; Jarrett, J. T.; Anderson, N. A.; Pullen, S. H.; Matthews, R. G.; Sension, R. J. Time-Resolved Spectroscopic Studies of B_{12} Coenzymes: The Identification of a Metastable Cob(III)alamin Photoproduct in the Photolysis of Methylcobalamin. *J. Am. Chem. Soc.* **1998**, *120*, 3597−3608.
(34) Shiang, J. J.; Walker, L. A., II; Anderson, N. A.; Cole, A. G.; Session, R. J. Time-Resolved Spectroscopic Studies of B_{12} Coenzymes: The Photolysis of Methylcobalamin Is Wavelength Dependent. *J. Phys. Chem. B* **1999**, *103*, 10532−10539.
(35) Cole, A. G.; Yoder, L. M.; Shiang, J. J.; Anderson, N. A.; Walker, L. A., II; Banaszak Holl, M. M.; Session, R. J. Time-Resolved Spectroscopic Studies of B_{12} Coenzymes: A Comparison of the Primary Photolysis Mechanism in Methyl-, Ethyl-, n-Propyl-, and 5′-Deoxyadenosylcobalamin. *J. Am. Chem. Soc.* **2002**, *124*, 434−441.
(36) Session, R. J.; Harris, D. A.; Cole, A. G. Time-Resolved Spectroscopic Studies of B_{12} Coenzymes: Comparison of the Influence of Solvent on the Primary Photolysis Mechanism and Geminate Recombination of Methyl-, Ethyl-, n-Propyl-, and 5′-Deoxyadenosylcobalamin. *J. Phys. Chem. B* **2005**, *109*, 21954−21962.
(37) Harris, D. A.; Stickrath, A. B.; Carroll, E. C.; Session, R. J. Influence of Environment on the Electronic Structure of Cob(III)-alamins: Time-Resolved Absorption Studies of the S_1 State Spectrum and Dynamics. *J. Am. Chem. Soc.* **2007**, *129*, 7578−7585.
(38) Stickrath, A. B.; Carroll, E. C.; Dai, X.; Harris, D. A.; Rury, A.; Smith, B.; Tang, K.; Wert, J.; Session, R. J. Solvent-Dependent Cage Dynamics of Small Nonpolar Radicals: Lessons from the Photodissociation and Geminate Recombination of Alkylcobalamins. *J. Phys. Chem. A* **2009**, *113*, 8513−8522.
(39) Peng, J.; Tang, K.-C.; McLoughlin, K.; Yang, Y.; Forgach, D.; Session, R. J. Ultrafast Excited-State Dynamics and Photolysis in Base-Off B_{12} Coenzymes and Analogues: Absence of the trans-Nitrogenous Ligand Opens a Channel for Rapid Nonradiative Decay. *J. Phys. Chem. B* **2010**, *114*, 12398−12405.
(40) Kohn, W.; Sham, L. J. Self-Consistent Equations Including Exchange and Correlation Effects. *Phys. Rev.* **1965**, *140*, A1133−A1138.
(41) Jones, R. O.; Gunnarsson, O. The density functional formalism, its applications and prospects. *Rev. Mod. Phys.* **1989**, *61*, 689−746.
(42) Kohn, W. Nobel Lecture: Electronic structure of matter - wave functions and density functionals. *Rev. Mod. Phys.* **1998**, *71*, 1253−1266.
(43) Parr, R. G.; Yang, W. *Density-Functional Theory of Atoms and Molecules*; Oxford University Press: Oxford, 1989.
(44) Runge, E.; Gross, E. K. U. Density-Functional Theory for Time-Dependent Systems. *Phys. Rev. Lett.* **1984**, *52*, 997−1000.
(45) Casida, M. E. Time-dependent density functional and response theory of molecular systems: Theory, computational methods and fuctionals. In *Recent Developments and Application of Modern Density Functional Theory*; Seminario, J. M., Ed.; Elsevier: Amsterdam, 1996; pp 391−439.
(46) Baerends, E. J.; Ricciardi, G.; Rosa, A.; van Gisergen, S. J. A. A DFT/TDDFT interpretation of the ground and excited states of porphyrin and porphyrazine complexes. *Coord. Chem. Rev.* **2002**, *230*, 5−27.

DOI: 10.1021/jp5120674
J. Phys. Chem. A 2015, 119, 3913−3928

(47) Dreuw, A.; Head-Gordon, M. Single-Reference ab Initio Methods for the Calculation of Excited States of Large Molecules. *Chem. Rev.* **2005**, *105*, 4009−4037.
(48) Dreuw, A. Quantum Chemical Methods for the Investigation of Photoinitiated Processes in Biological Systems: Theory and Applications. *ChemPhysChem* **2006**, *7*, 2259−2274.
(49) Jaworska, M.; Lodowski, P.; Andruniów, T.; Kozlowski, P. M. Photolysis of methylcobalamin: identification of the relevant excited states involved in Co−C bond scission. *J. Phys. Chem. B* **2007**, *111*, 2419−2422.
(50) Lodowski, P.; Jaworska, M.; Andruniów, T.; Kumar, M.; Kozlowski, P. M. Photodissociation of Co−C bond in methyl- and ethylcobalamin: an insight from TD-DFT calculations. *J. Phys. Chem. B* **2009**, *113*, 6898−6909.
(51) Kornobis, K.; Kumar, N.; Lodowski, P.; Jaworska, M.; Piecuch, P.; Lutz, J. J.; Wong, B. M.; Kozlowski, P. M. Electronic structure of the S_1 state in methylcobalamin: Insight from CASSCF/MC-XQDPT2, EOM-CCSD, and TD-DFT calculations. *J. Comput. Chem.* **2013**, *34*, 987−1004.
(52) Jones, A. R.; Woodward, J. R.; Scrutton, N. S. Continuous Wave Photolysis Magnetic Field Effect Investigations with Free and Protein-Bound Alkylcobalamins. *J. Am. Chem. Soc.* **2009**, *131*, 17246−17253.
(53) Lodowski, P.; Jaworska, M.; Andruniów, T.; Garabato, B.; Kozlowski, P. Mechanism of Co-C Bond Photolysis in the Base-on Form of Methylcobalamin. *J. Phys. Chem. A* **2014**, DOI: 10.1021/jp508513p.
(54) Landau, L. D. Zur theorie der energieubertagung. II. *Phys. Soviet Union* **1932**, *2*, 46−51.
(55) Zener, C. Non-Adiabatic Crossin of Energy Levels. *Proc. R. Soc. London, Ser. A* **1932**, *137*, 696−702.
(56) Kasper P. Jensen, K. P.; Ryde, U. Cobalamins uncovered by modern electronic structure calculations. *Coord. Chem. Rev.* **2009**, *253*, 769−778.
(57) Marsh, E. N. G.; Meléndez, G. D. R. Adenosylcobalamin enzymes: Theory and experiment begin to converge. *Biochim. Biophys. Acta* **2012**, *1824*, 1154−1164.
(58) Klamt, A.; Schüürmann, G. COSMO: A new approach to dielectric screening in solvents with explicit expressions for the screening energy and its gradient. *J. Chem. Soc., Perkin Trans. 2* **1993**, 799−805.
(59) Schäfer, A.; Klamt, A.; Sattel, D.; Lohrenz, J.; Eckert, F. COSMO Implementation in TURBOMOLE: Extension of an efficient quantum chemical code towards liquid systems. *Phys. Chem. Chem. Phys.* **2000**, *2*, 2187−2193.
(60) Becke, A. D. Density functional exchange energy approximation with correct asymptotic behavior. *Phys. Rev. A* **1988**, *38*, 3098−3100.
(61) Perdew, J. P. Density-functional approximation for the correlation energy of the inhomogeneous electron gas. *Phys. Rev. B* **1986**, *33*, 8822−8824.
(62) *TURBOMOLE V5.10 2008, a development of University of Karlsruhe and Forschungszentrum Karlsruhe GmbH, 1989−2007*; TURBOMOLE GmbH, since 2007; available from http://www.turbomole.com.
(63) Weigend, F.; Häser, M.; Patzelt, H.; Ahlrichs, R. RI-MP2: Optimized Auxiliary Basis Sets and Demonstration of Efficiency. *Chem. Phys. Lett.* **1998**, *294*, 143−152.
(64) Sierka, M.; Hogekamp, A.; Ahlrichs, R. Fast evaluation of the Coulomb potential for electron densities using multipole accelerated resolution of identity approximation. *J. Chem. Phys.* **2003**, *118*, 9136−9148.
(65) Eichkorn, K.; Weigend, F.; Treutler, O.; Ahlrichs, R. Auxiliary basis sets for main row atoms and transition metals and their use to approximate Coulomb potentials. *Theor. Chem. Acc.* **1997**, *97*, 119−124.
(66) Jensen, K. P.; Ryde, U. Theoretical Prediction of the Co−C Bond Strength in Cobalamins. *J. Phys. Chem. A* **2003**, *107*, 7539−7545.
(67) Jensen, K. P.; Ryde, U. How the Co−C bond is cleaved in coenzyme B_{12} enzymes: A theoretical study. *J. Am. Chem. Soc.* **2005**, *127*, 9117−9128.
(68) Dölker, N.; Morreale, A.; Maseras, F. Computational study on the difference between the Co-C bond dissociation energy in methylcobalamin and adenosylcobalamin. *J. Biol. Inorg. Chem.* **2005**, *10*, 509−517.
(69) Kuta, J.; Patchkovskii, S.; Zgierski, M. Z.; Kozlowski, P. M. Performance of DFT in modeling electronic and structural properties of cobalamins. *J. Comput. Chem.* **2006**, *27*, 1429−1437.
(70) Kozlowski, P. M.; Kuta, J.; Galezowski, W. Reductive cleavage mechanism of methylcobalamin: elementary steps of Co−C bond breaking. *J. Phys. Chem. B* **2007**, *111*, 7638−7645.
(71) Kozlowski, P. M.; Kumar, M.; Piecuch, P.; Li, W.; Bauman, N. P.; Hansen, J. A.; Lodowski, P.; Jaworska, M. The Cobalt−Methyl Bond Dissociation in Methylcobalamin: New Benchmark Analysis Based on Density Functional Theory and Completely Renormalized Coupled-Cluster Calculations. *J. Chem. Theory Comput.* **2012**, *8*, 1870−1894.
(72) Kornobis, K.; Kumar, N.; Wong, B. M.; Lodowski, P.; Jaworska, M.; Andruniów, T.; Ruud, K.; Kozlowski, P. M. Electronically Excited States of Vitamin B12: Benchmark Calculations Including Time-Dependent Density Functional Theory and Correlated ab Initio Methods. *J. Phys. Chem. A* **2011**, *115*, 1280−1292.
(73) Grimme, S. Semiempirical GGA-type density functional constructed with a long-range dispersion correction. *J. Comput. Chem.* **2006**, *27*, 1787−1799.
(74) Kobylianskii, I. J.; Widner, F. J.; Kräutler, B.; Chen, P. Co−C Bond Energies in Adenosylcobinamide and Methylcobinamide in the Gas Phase and in Silico. *J. Am. Chem. Soc.* **2013**, *135*, 13648−13651.
(75) Dong, S.; Padmakumar, R.; Banerjee, R.; Spiro, T. G. Co-C force constants from resonance Raman spectra of alkylcobalamins: insensitivity to dimethylbenzylimidazole coordination. *Inorg. Chim. Acta* **1998**, *270*, 392−398.
(76) Reed, A. E.; Weinstock, R. B.; Weinhold, F. Natural population analysis. *J. Chem. Phys.* **1985**, *83*, 735−746.
(77) Kumar, M.; Kozlowski, P. M. A Biologically Relevant Co1+···H Bond: Possible Implications in the Protein-Induced Redox Tuning of Co2+/Co1+ Reduction. *Angew. Chem., Int. Ed.* **2011**, *50*, 8702−8705.
(78) Kepp, K. P. O_2 Binding to Heme is Strongly Facilitated by Near-Degeneracy of Electronic States. *ChemPhysChem* **2013**, *14*, 3551−3558.
(79) Kepp, K. P. Co−C Dissociation of Adenosylcobalamin (Coenzyme B_{12}): Role of Dispersion, Induction Effects, Solvent Polarity, and Relativistic and Thermal Corrections. *J. Phys. Chem. A* **2014**, *118*, 7104−7117.
(80) Harvey, J. N. Understanding the kinetics of spin-forbidden chemical reactions. *Phys. Chem. Chem. Phys.* **2007**, *9*, 331−343.
(81) Lower, S. K.; El-Sayed, M. A. The Triplet State and Molecular Electronic Processes in Organic Molecules. *Chem. Rev.* **1966**, *66*, 199−241.
(82) El-Sayed, M. A. The Triplet State: Its Radiative and Nonradiative Properties. *Acc. Chem. Res.* **1968**, *1*, 8−16.
(83) Marian, Ch. M. Spin−orbit coupling and intersystem crossing in molecules. *Wiley Interdiscip. Rev.: Comput. Mol. Sci.* **2011**, *1*, 1−17 DOI: 10.1002/wcms.83.
(84) Cannizzo, A.; Blanco-Rodriguez, A. M.; El Nahhas, A.; Šebera, J.; Záliš, S.; Vlček, A., Jr.; Chergui, M. Femtosecond Fluorescence and Intersystem Crossing in Rhenium(I) Carbonyl-Bipyridine Complexes. *J. Am. Chem. Soc.* **2008**, *130*, 8967−8974.

DOI: 10.1021/jp5120674
J. Phys. Chem. A 2015, 119, 3913−3928